A method for the continuous monitoring of reactivity in subcritical source-driven systems

# A METHOD FOR THE CONTINUOUS MONITORING OF REACTIVITY IN SUBCRITICAL SOURCE-DRIVEN SYSTEMS

S. Dulla, M. Nervo, P. Ravetto

*Politecnico di Torino, Dipartimento Energia*
*Corso Duca degli Abruzzi, 24 - 10129 Torino (Italy)*
*sandra.dulla@polito.it, marta.nervo@polito.it, piero.ravetto@polito.it*
*Tel. +39 011 090 4416, Fax. +39 011 090 4499*

**Abstract**

The reactivity monitoring in subcritical accelerator-driven systems is a key aspect for the development of this technology. In this work, an inverse method for the determination of the system reactivity from the analysis of flux and power signals, based on the point kinetic approach, is applied to source-driven systems. The features of the algorithm specific to the application to subcritical assemblies are identified, and the sensitivity to the integral parameters characterizing the system is discussed. The technique is applied to different transient situations, simulated by neutronic codes adopting point kinetics and multigroup diffusion, and its accuracy in the presence of localized spatial and spectral phenomena is assessed. Different approaches for the reduction of the uncertainties introduced by the experimental noise are proposed and compared.

*Key words:* on-line reactivity monitoring, point kinetics, stable period, subcritical source-driven systems

## 1 Introduction

On-line monitoring is a high-priority task to guarantee the safe operation of nuclear power systems. In particular, it is a crucial aspect in the operation of Accelerator-Driven Systems (ADS) to keep under control the subcriticality margin and to promptly detect potentially dangerous situations. In the past decade several experimental campaigns have been performed considering different subcritical configurations to test and assess various reactivity reconstruction techniques (Sjöstrand, 1956; Salvatores et al., 1996; Persson et al., 2005). However, most experiments are based on the analysis of the system response following a source trip and, therefore, they are not

suitable for continuous monitoring. However, they can provide accurate reference values of the subcriticality level. More recently, the so-called current-to-flux ratio method has been proposed as a suitable on-line reactivity monitoring technique for subcritical facilities (Becares et al., 2013; Cao et al., 2013). The method relies on the monitoring of the ratio between the beam current intensity driving the neutron source and the neutron flux measurement signal.

In the framework of on-line monitoring techniques investigations, a novel method has been recently developed and assessed for source-free systems (Dulla et al., 2014b). The present work illustrates the extension of that algorithm to source-driven systems. The aim of this technique is to detect the distance of the system from criticality in real time from the interpretation of neutron flux measurements. As for the current-to-flux method, it requires some information on a reference system, which is supposed to be available from independent measurements. The method is based on the point kinetic model, for which it is possible to mathematically establish a relationship between the state variables (power and neutron precursor effective concentrations) and the inverse of the stable period of the multiplying system, i.e. the fundamental eigenvalue of the time-dependent model; the reactivity can then be determined at each instant through the inhour relationship. The information on the stable period is derived from the instantaneous value of the state variables and thus the value of the retrieved reactivity corresponds to the instantaneous situation of the evolving system.

In the following sections the description of the method derivation is presented and the assessment of the method is carried out by simulating power signals as the direct solution of the point kinetic model. The effect of experimental noise is then investigated in order to analyse the robustness of the method. The algorithm is then applied to the interpretation of flux signals generated by a more realistic reactor model to investigate spatial and spectral effects. The results obtained allow to consider the method adequate and promising for the application to on-line reactivity monitoring of sucbritical nuclear systems driven by an external neutron source.

## 2 Fundamentals of the method

The present section extends the method recently developed for source-free systems (Dulla et al., 2014b) for the application to source-driven systems. The method proposed is based on the point kinetic reactor model (Akcasu et al., 1971) and, for the sake of simplicity, to illustrate the philosophy of the technique, the system of ordinary first-order differential equations is written down considering only a single

neutron precursor family, the model easily being extended to more families:

$$\begin{cases} \dot{P}(t) = \dfrac{\rho - \beta}{\Lambda} P(t) + \lambda C(t) + S(t) \\ \\ \dot{C}(t) = \dfrac{\beta}{\Lambda} P(t) - \lambda C(t). \end{cases} \tag{1}$$

The quantity $P$ is the neutron flux amplitude (or system power), $C$ is the effective delayed neutron precursor concentration and $S$ the effective external source. The parameters $\beta$, $\Lambda$ and $\lambda$ are the effective delayed neutron fraction, the effective prompt neutron generation time and the delayed neutron precursor decay constant, respectively. Dotted quantities denote time derivatives. The quantities $\beta$ and $\Lambda$ characterizing the physical system should be known from independent measurements (e.g., Pepyolyshev (2008); Kuramoto et al. (2007)).

The method is derived in order to obtain a tool capable to reconstruct the evolution of the reactivity during a transient started in a system initially in a normal steady-state operation under the injection of a constant source $S_0$. It is supposed that the information on the evolution of the system amplitude can be retrieved by direct neutron flux measurements. The initial state is characterized by the following relationship between the initial source intensity and the power, which can be determined by the steady-state version of Eq. (1):

$$P_0 = -\frac{S_0 \Lambda}{\rho_0}. \tag{2}$$

The reactivity $\rho_0$ should also be known from measurements on the initial reference system. Therefore, if the initial power is available by direct measurements of the neutron flux, the effective source $S_0$ acting on the system is also available. The precursor concentration can be obtained by time integration of the second equation in system (1):

$$C(t) = C(0)\exp(-\lambda t) + \frac{\beta}{\Lambda}\int_0^t P(t')\exp(-\lambda(t-t'))dt' = C(0)\exp(-\lambda t) + \frac{\beta}{\Lambda} I(t), \tag{3}$$

where the intial equilibrium condition of the neutron precursor concentration is given by the relationship with the initial source level:

$$C_0 = -\frac{S_0 \beta}{\lambda \rho_0}. \tag{4}$$

During the operation of the system, unexpected events may change the total reactivity inducing a transient characterized by a perturbation $\rho_p$, so that the total reactivity $\rho$ acting on the system is the sum of $\rho_p$ and the initial, negative, reactivity $\rho_0$. The aim of the on-line monitoring is to estimate the reactivity $\rho$ at each instant.

The reactivity reconstruction procedure can be developed by resorting to the mathematical properties of the solution of system (1), assuming a given reactivity level

$\rho$. The point kinetic model can be rewritten in matrix form as:

$$\frac{d\,|X(t)\rangle}{dt} = \hat{A}\,|X(t)\rangle + |S(t)\rangle\,, \tag{5}$$

where the unknown (column) state vector, defined by the power $P$ and the effective delayed neutron concentration $C$, the source vector and the system characteristic matrix are introduced as:

$$|X(t)\rangle = \left|\begin{matrix} P(t) \\ C(t) \end{matrix}\right\rangle; \quad |S(t)\rangle = \left|\begin{matrix} S(t) \\ 0 \end{matrix}\right\rangle; \quad \hat{A} = \begin{pmatrix} \dfrac{\rho-\beta}{\Lambda} & \lambda \\ \dfrac{\beta}{\Lambda} & -\lambda \end{pmatrix}. \tag{6}$$

The fully analytical form of the solution can be retrieved solving the eigenvalue problem:

$$\left\|\hat{A} - \omega\hat{I}\right\| = 0, \tag{7}$$

which can be cast into the form of the classic inhour equation:

$$\rho = \omega\Lambda + \frac{\omega\beta}{\omega+\lambda}, \tag{8}$$

leading to two real, distinct solutions for subcritical systems, $\omega_1$ and $\omega_2$, such that $0 > \omega_1 > -\lambda$ and $\omega_2 < -\lambda$. The corresponding (column) eigenvectors of matrix $\hat{A}$ can be explicitly written and they constitute the most suitable basis to express the state vector (Ravetto, 1997). However, they are not orthogonal, hence the adjoint (row) vectors are needed to be able to decouple the equations for the components of the solution along each eigenvector; it is rather easy to find out the following expressions for the un-normalized direct and adjoint eigenvectors:

$$|U_k\rangle = \left|\begin{matrix} 1 \\ \dfrac{\beta/\Lambda}{\omega_k+\lambda} \end{matrix}\right\rangle; \quad \langle U_h| = \left\langle 1 \quad \frac{\lambda}{\omega_h+\lambda}\right|; \quad h,k = 1,2. \tag{9}$$

At last, the general solution can be written as a superposition of the response to the initial state and of the convolution-type response to the source injection:

$$|X(t)\rangle = \sum_{k=1}^{2}\left[\frac{\langle U_k|X(0)\rangle}{\langle U_k|U_k\rangle}\exp(\omega_k t) + \int_0^t dt' \frac{\langle U_k|S(t')\rangle}{\langle U_k|U_k\rangle}\exp(\omega_k(t-t'))\right]|U_k\rangle\,. \tag{10}$$

Let us now suppose that the source is kept constant and equal to the stationary value $S_0$ after the introduction of the perturbation. The convolution term can thus be evaluated, obtaining:

$$|X(t)\rangle = \sum_{k=1}^{2}\left[\frac{\langle U_k|X(0)\rangle}{\langle U_k|U_k\rangle}\exp(\omega_k t) + \frac{\langle U_k|S_0\rangle}{\langle U_k|U_k\rangle}\frac{1}{\omega_k}\left(\exp(\omega_k t)-1\right)\right]|U_k\rangle\,. \tag{11}$$

The power evolution expression is obtained by simply taking the first component of the state vector in Eq. (11).

The procedure is based on a general approach to the analysis of dynamical systems (Krilov, 1931), which can be applied to the point kinetic model for nuclear reactors (Corno et al., 1986) and has been recently assessed as a tool for experimental reactivity determination in source-free systems (Dulla et al., 2014b). If one assumes that the reactivity would be maintained at the instantaneous value $\rho$, the system is expected to reach an asymptotic state for large values of the time, say $t^*$. However, unlike what happens for source-free systems, both eigenstates shall contribute to the asymptotic regime, explicitly, from Eq. (11):

$$P(t^*) \cong \left[\frac{\langle U_1|X(0)\rangle}{\langle U_1|U_1\rangle} + \frac{\langle U_1|S_0\rangle}{\langle U_1|U_1\rangle}\frac{1}{\omega_1}\right]\exp(\omega_1 t^*) - \sum_{k=1}^{2}\frac{\langle U_k|S_0\rangle}{\langle U_k|U_k\rangle}\frac{1}{\omega_k}. \tag{12}$$

At any times $t << t^*$ one can evaluate the asymptotic situation that would be reached if the state at such time were assumed as initial state, which must be the same as the one obtained by Eq. (12):

$$P(t^*) \cong \left[\frac{\langle U_1|X(t)\rangle}{\langle U_1|U_1\rangle} + \frac{\langle U_1|S_0\rangle}{\langle U_1|U_1\rangle}\frac{1}{\omega_1}\right]\exp(\omega_1(t^*-t)) - \sum_{k=1}^{2}\frac{\langle U_k|S_0\rangle}{\langle U_k|U_k\rangle}\frac{1}{\omega_k}. \tag{13}$$

The comparison of Eqs. (12) and (13) allows to eliminate the terms involving both eigenvalues:

$$\left[P(t) + \frac{\lambda}{\omega_1+\lambda}C(t) + \frac{1}{\omega_1}S_0\right]\exp(-\omega_1 t) = \langle U_1|X(0)\rangle + \frac{1}{\omega_1}\langle U_1|S_0\rangle = \text{const.} \tag{14}$$

Taking the time derivative of Eq. (14), the time constant term is eliminated and it possible to obtain a relationship providing the instantaneous connection between the power $P$ and the effective delayed neutron precursors $C$ and the fundamental eigenvalue of the system $\omega_1$:

$$\left[\frac{\dot{P}(t)}{S_0}\right] - \omega_1\left[\frac{P(t)}{S_0}\right] + \frac{\lambda}{\omega_1+\lambda}\left[\frac{\dot{C}(t)}{S_0}\right] - \omega_1\frac{\lambda}{\omega_1+\lambda}\left[\frac{C(t)}{S_0}\right] - 1 = H(\beta,\Lambda,\rho_0;\omega_1) = 0. \tag{15}$$

This algorithm meets the initial objective of the work, since it allows to determine the time eigenvalue $\omega_1$, inverse of the stable period, from experimental observables $P$, $\dot{P}$, $C$ (from Eq. (3)) and $\dot{C}$ (from the second of Eqs. (1)). Through the inhour equation (8), the "experimental" value of the reactivity, $\rho_{exp}$, can be reconstructed at all time instants from the value of the fundamental eigenvalue of the system, $\omega_1$, which is the largest root of the algebraic second-degree equation (15) shown above. It is worth to remark that the value of the instantaneous period corresponds to the instantaneous state of the system. All the time frequencies appear in the system behavior at any time and the solution of the inhour equation (8) allows to identify all of them; the selection of the largest root of (8) corresponds to the inverse of the

stable period that leads to the estimation of the system reactivity.

For the application of this method to subcritical source-driven system, the initial subcriticality level has to be independently measured, in order to be able to calibrate the value of the effective source. The algorithm then provides the estimation of the total reactivity of the system $\rho$, allowing to measure the subcriticality margin and to detect the possible occurrence of accidental sequences even when the system becomes supercritical.

The reactivity reconstruction algorithm can be easily generalized to any number of delayed neutron families $M$, providing the multiple-family counterpart of Eq. (15) in the form:

$$\dot{P}(t) - \omega_1 P(t) + S_0 + \sum_{i=1}^{M} \frac{\lambda_i}{\omega_1 + \lambda_i} \left[ \dot{C}_i(t) - \omega_1 C_i(t) \right] = 0. \tag{16}$$

The quality of the reactivity prediction is influenced by the adopted number of delayed neutron families, especially at times comparable to the characteristic decay times of the delayed neutron precursors (Dulla et al., 2014b,c).

## 3 General features of the method and sensitivity to integral parameters

In order to validate and to assess the performance of the method, in place of real experimental values, the power signal to be applied within the algorithm is generated by numerical evaluations. At first a point kinetic model is used to generate the power histories. It is clear that the exact reactivity is obviously re-obtained, being the inverse interpretation procedure based on the same model. Errors may be introduced by the use of discrete formulae to compute derivatives and integrals, since in real measurements the power signal is acquired only at discrete time values. A parametric analysis on the dimension of the time discretization has proven that the performances of the method are satisfactory even using large values of the sampling time mesh, even up to values of the order of $10^{-2}$ s, as it was previously verified in the application to source-free reactors (Dulla et al., 2014b).

It is also interesting and important to investigate how the accuracy of the integral parameters (effective delayed neutron fractions and mean prompt generation time) affects the reactivity prediction, since their values are also obtained from experimental measurements. In addition, in the case of a source-driven system the uncertainty related to the measurement of the initial reactivity $\rho_0$ has also to be investigated. For the evaluation of the sensitivity coefficients of $\rho$ for $\beta$ ($S_\beta$), $\Lambda$ ($S_\Lambda$) and $\rho_0$ ($S_{\rho_0}$), one can directly refer to Eq. (8), obtaining:

$$S_\beta = \left| \frac{\delta\rho}{\delta\beta/\beta} \right| = \left| \frac{\omega_1}{\omega_1 + \lambda} + \left[ \Lambda + \frac{\beta\lambda}{(\omega_1 + \lambda)^2} \right] \frac{\partial \omega_1}{\partial \beta} \right| \beta, \tag{17}$$

$$S_\Lambda = \left| \frac{\delta\rho}{\delta\Lambda/\Lambda} \right| = \left| \omega_1 + \left[ \Lambda + \frac{\beta\lambda}{(\omega_1+\lambda)^2} \right] \frac{\partial\omega_1}{\partial\Lambda} \right| \Lambda, \tag{18}$$

and

$$S_{\rho_0} = \left| \frac{\delta\rho}{\delta\rho_0} \right| = \left| \left[ \Lambda + \frac{\beta\lambda}{(\omega_1+\lambda)^2} \right] \frac{\partial\omega_1}{\partial\rho_0} \right|. \tag{19}$$

The partial derivatives of the fundamental eigenvalue with respect to $\beta$, $\Lambda$ and $\rho_0$ are obtained by derivation of the implicit formula (15), as:

$$\begin{gathered} \frac{\partial\omega_1}{\partial\beta} = -\frac{\dfrac{\partial H(\beta,\Lambda,\rho_0;\omega_1)}{\partial\beta}}{\dfrac{\partial H(\beta,\Lambda,\rho_0;\omega_1)}{\partial\omega_1}}, \qquad \frac{\partial\omega_1}{\partial\Lambda} = -\frac{\dfrac{\partial H(\beta,\Lambda,\rho_0;\omega_1)}{\partial\Lambda}}{\dfrac{\partial H(\beta,\Lambda,\rho_0;\omega_1)}{\partial\omega_1}}, \\ \frac{\partial\omega_1}{\partial\rho_0} = -\frac{\dfrac{\partial H(\beta,\Lambda,\rho_0;\omega_1)}{\partial\rho_0}}{\dfrac{\partial H(\beta,\Lambda,\rho_0;\omega_1)}{\partial\omega_1}}, \end{gathered} \tag{20}$$

$$\frac{\partial H(\beta,\Lambda,\rho_0;\omega_1)}{\partial\beta} = \frac{\lambda}{\Lambda}\left( \frac{P}{\lambda+\omega_1} - I(t) \right), \tag{21}$$

$$\frac{\partial H(\beta,\Lambda,\rho_0;\omega_1)}{\partial\Lambda} = \frac{\lambda\beta}{\Lambda^2}\left( -\frac{P}{\lambda+\omega_1} + I(t) \right) + \frac{\rho_0 P_0}{\Lambda^2}, \tag{22}$$

$$\frac{\partial H(\beta,\Lambda,\rho_0;\omega_1)}{\partial\rho_0} = \frac{P_0}{\Lambda}, \tag{23}$$

$$\frac{\partial H(\beta,\Lambda,\rho_0;\omega_1)}{\partial\omega_1} = -P\left( 1 + \frac{\lambda\beta}{\Lambda(\lambda+\omega_1)^2} \right). \tag{24}$$

It is possible to establish that in general the value of the mean effective prompt generation time has little effect on the sensitivity of the method to the accuracy of $\Lambda$ itself, therefore the method can perform satisfactorily for both fast and thermal systems. This can be easily verified by substitution of Eq. (22) into Eq. (18). Considering Eqs. (18) and (22) one can also conclude that $S_\Lambda$ is little affected by the time instant considered in the transient. This sensitivity parameter increases with the level of subcriticality of the system, as can be seen by Table 1, where also the effect of the effective delayed neutron fraction is shown, although it is rather small.

The results of the analysis of the sensitivity with respect to the delayed neutron fraction are summarized Fig. 1. The parameter $S_\beta$ has a linear behavior with respect to the values of $\beta$ itself, and it is found that such trend is not significantly affected by the values of time instants, reactivity and mean generation time. It is worth recalling the attention upon the fact that usual measurements of effective delayed neutron fraction and mean prompt generation time yield results with associated uncertainties of the order of some percents (Baeten et al., 2001).

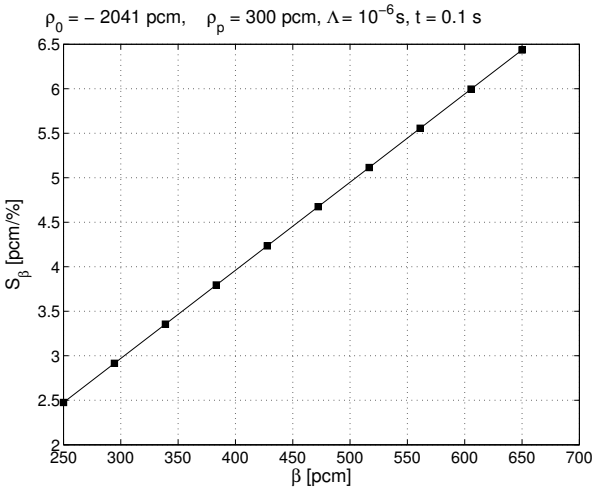


Figure 1. Behavior of $S_\beta$ with respect to the effective delayed neutron fraction $\beta$ at time 0.1 s ($\beta = 650$ pcm, $\rho = -1741$ pcm, $\Lambda = 10^{-6}$ s).

Table 1
Effect on the sensitivity associated to the effective prompt generation time due to various values of $\beta$ and $\rho_p$.

| | | $\beta = 250$ pcm | $\beta = 650$ pcm |
|---|---|---|---|
| $\rho_0$ [pcm] | $\rho_p$ [pcm] | $S_\Lambda$ [pcm/%] | $S_\Lambda$ [pcm/%] |
| $-3093$ | $-100$ | 34.4 | 38.4 |
| | 100 | 32.4 | 36.4 |
| | 200 | 31.4 | 35.4 |
| $-2041$ | $-100$ | 23.9 | 27.9 |
| | 100 | 21.9 | 25.9 |
| | 200 | 20.9 | 24.9 |
| $-1010$ | $-100$ | 13.6 | 17.6 |
| | 100 | 11.6 | 15.6 |
| | 200 | 10.6 | 14.6 |

Substituting Eq. (23) into Eq. (19), one finds that the sensitivity to the initial reactivity can be simply determined by the ratio between the initial power level and the power at each instant along the transient:

$$S_{\rho_0} = \frac{\partial \rho}{\partial \rho_0} = \frac{P_0}{P}. \tag{25}$$

This relationship denotes that the accuracy of the prediction is reduced when the power level measured is decreased. This aspect is certainly relevant for the safety

assessment of the system, being related to the reliability of the measurement of the subcriticality level.

## 4 Experimental noise analysis

To validate the robustness of the method for application to reactivity monitoring, the effect of the experimental noise must be investigated and noise mitigation techniques must be studied. The noise associated to the power signal itself affects the reactivity prediction process in various manners. Considering formula (15), one may observe that the experimental noise of the power signals indirectly affects significantly the derivative of the power and of the delayed neutron precursor concentrations.

The evaluation of the power derivative can be carried out taking advantage of well-assessed algorithms to differentiate noisy functions. In the present work, the derivative is evaluated after reducing the noisy component through the minimization of a proper functional of the original signal (Chartrand, 2011). As shown in the following, this differentiation algorithm proves to yield satisfactory results, except at the very beginning of the transient following a reactivity perturbation.

The derivative of the effective precursor concentration can be obtained by the second equation of the the point kinetic system (1). This expression is directly affected by the noise associated to the power signal measurements. Alternatively, the value of the derivative of the neutron precursor concentration can be obtained by standard finite differences applied to the discrete values of $C$ obtained through Eq. (3): this technique is beneficial and leads to some reduction of the noise effect in the reactivity prediction. This is due to the fact that the neutron precursor concentration is obtained by an integral functional of the power: such integration procedure provides a result that is less affected by noise and, therefore, a better estimation of the derivative is retrieved.

To mitigate the experimental noise, usually a hardware low-pass filter is used on the signal output from neutron detectors (Becares et al., 2013). In addition, one may also consider the introduction of a data filtering process to improve the quality of the information for the reactivity reconstruction. In this work two approaches, the Moving Mean Filter (MMF) (Savitzky and Golay, 1964) and the Kalman Filter (KF) (Kalman, 1960), are applied and their performances are compared.

Since no actual experimental measurements for transients in a subcritical assembly are available, a noise component is introduced into the computed signals used for the interpretation: the value of the noisy power signal is generated at each detection time by numerically sampling a uniform statistical distribution of width $\delta$ centered around the original computed value. The quantity $\delta$ is a measure of the dispersion

of the experimental data. By repeating the procedure at each sampling time, a full transient history can be generated, which can be considered as representative of the experimental measurements obtained in the real case.

The sampling of all power histories generated with this procedure allows a statistical analysis in a Monte Carlo fashion. The reactivity is obtained applying the reconstruction algorithm at each time instant for each power history, and the corresponding sample average and standard deviation can be evaluated. This analysis allows to get useful information on how the statistical uncertainty associated to the power signal can influence the reactivity accuracy prediction, in terms of mean value and dispersion of the reactivity.

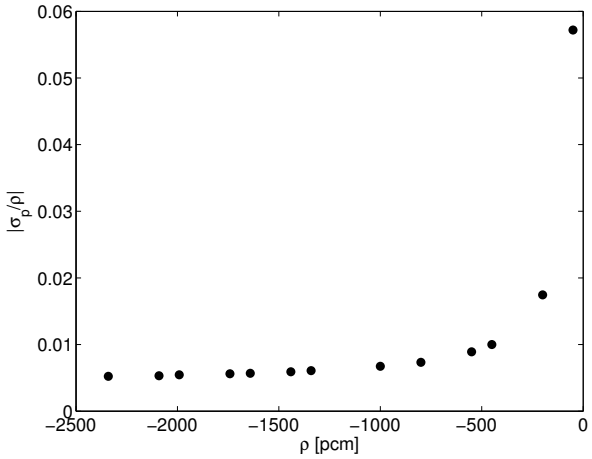


Figure 2. Behaviour of the ratio between the standard deviation and the total reactivity, as a function of the reactivity itself. A white noise is assumed ($\delta = 1\%$) and the signal is interpreted using a sample history with time intervals of $10^{-5}$ s. The results are taken at $10^{-2}$ s after the insertion of the perturbation.

Tables 2 through 5 present some results of the statistical analysis. For all calculations a sampling interval of $10^{-5}$ s is adopted. Two different values of the reactivity injection $\rho_p$ are considered to induce the transients. Different values of the amplitude $\delta$ of the signal dispersion are considered. The values of the kinetic parameters adopted for these evaluations are: $\beta = 650$ pcm, $\Lambda = 1$ $\mu$s and $\lambda = 0.1$ s$^{-1}$.

Results reported in Table 2 have been obtained introducing no filtering to the noisy power data, and provide a reference to appreciate the efficacy of the different filters in reducing the statistical disturbance. To better understand the behavior of the standard deviations appearing in Table 2, it is useful to consider Fig. 2, where the ratio of the standard deviation to the total reactivity is plotted against the reactivity itself. The graph shows that the statistical dispersion increases when approaching the critical state, while it stabilizes for subcriticality levels lower than 1000 pcm. This trend is characteristics of how the statistical error on the input data is processed by the reactivity reconstruction algorithm, while the amount of dispersion can be reduced by the use of a proper filtering technique.

Table 2
Statistical analysis of the effect of the power signal noise. The transient is induced by an insertion of $\rho_p$ reactivity. $\langle \rho_{p,exp} \rangle$ denotes the sample average of the measured distance between the experimental reactivity $\rho_{exp}$ and the reference configuration $\rho_0 = -2041$ pcm; $\sigma_\rho$ is the corresponding standard deviation. Ten thousand power histories are considered.

| | | $\rho_p = 50$ pcm | | $\rho_p = 300$ pcm | |
|---|---|---|---|---|---|
| $\delta$ [%] | $t$ [s] | $\langle \rho_{p,exp} \rangle$ [pcm] | $\sigma_\rho$ [pcm] | $\langle \rho_{p,exp} \rangle$ [pcm] | $\sigma_\rho$ [pcm] |
| 1 | $1.0E-04$ | 45.9 | 10.8 | 271.9 | 9.9 |
| | $5.0E-04$ | 50.0 | 10.8 | 300.0 | 9.9 |
| | $7.5E-04$ | 49.8 | 10.7 | 300.0 | 9.9 |
| | $1.0E-03$ | 50.0 | 10.8 | 300.1 | 9.6 |
| | $1.0E-02$ | 49.8 | 10.9 | 300.0 | 9.8 |
| 3 | $1.0E-04$ | 45.4 | 32.3 | 271.5 | 29.6 |
| | $5.0E-04$ | 49.7 | 32.7 | 299.7 | 29.3 |
| | $7.5E-04$ | 49.8 | 32.7 | 299.1 | 29.2 |
| | $1.0E-03$ | 50.0 | 32.0 | 299.7 | 29.2 |
| | $1.0E-02$ | 49.7 | 32.4 | 299.2 | 29.5 |
| 5 | $1.0E-04$ | 44.6 | 54.0 | 270.7 | 49.4 |
| | $5.0E-04$ | 49.0 | 54.0 | 299.1 | 48.9 |
| | $7.5E-04$ | 48.0 | 53.8 | 298.2 | 48.7 |
| | $1.0E-03$ | 49.0 | 53.8 | 299.1 | 48.7 |
| | $1.0E-02$ | 48.1 | 54.4 | 298.3 | 49.3 |
| 10 | $1.0E-04$ | 41.0 | 108.5 | 267.5 | 99.2 |
| | $5.0E-04$ | 45.8 | 108.4 | 296.2 | 98.2 |
| | $7.5E-04$ | 43.8 | 108.0 | 294.4 | 97.8 |
| | $1.0E-03$ | 45.7 | 108.0 | 296.1 | 97.8 |
| | $1.0E-02$ | 43.9 | 109.3 | 294.5 | 98.9 |

To produce the results of Tables 3 and 4, a MMF has been introduced to process the detector (power) signals before the reactivity reconstruction analysis. The filtering allows to reduce the noise of the result, thus improving the quality of the reactivity prediction. Thus, as expected, Tables 3 and 4 show that the standard deviations are smaller than in Table 2. The comparisons of Tables 3 and 4 also illustrates that the improvement that can be obtained adopting 11 data points instead of 5 in the MMF algorithm is rather limited, providing a guideline for the identification of the most suitable data span to be introduced in the filter. This aspect is rather relevant, since

Table 3
Results of statistical analysis using a Moving Mean Filter over a 5 point span to process the signal affected by noise before applying the reactivity reconstruction method. The transient is induced by an insertion of $\rho_p$ reactivity. $\langle \rho_{p,exp} \rangle$ denotes the sample average of the measured distance between the experimental reactivity $\rho_{exp}$ and the reference configuration $\rho_0 = -2041$ pcm; $\sigma_\rho$ is the corresponding standard deviation. Ten thousand power histories are considered.

| | | $\rho_p = 50$ pcm | | $\rho_p = 300$ pcm | |
|---|---|---|---|---|---|
| $\delta$ [%] | $t$ [s] | $\langle \rho_{p,exp} \rangle$ [pcm] | $\sigma_\rho$ [pcm] | $\langle \rho_{p,exp} \rangle$ [pcm] | $\sigma_\rho$ [pcm] |
| 1 | $1.0E-04$ | 45.6 | 6.4 | 270.3 | 5.9 |
| | $5.0E-04$ | 50.1 | 6.5 | 299.9 | 5.8 |
| | $7.5E-04$ | 50.0 | 6.5 | 299.9 | 5.9 |
| | $1.0E-03$ | 49.9 | 6.5 | 300.1 | 5.8 |
| | $1.0E-02$ | 49.9 | 6.9 | 300.0 | 6.2 |
| 3 | $1.0E-04$ | 45.6 | 19.5 | 270.1 | 17.7 |
| | $5.0E-04$ | 49.5 | 19.3 | 299.8 | 17.8 |
| | $7.5E-04$ | 49.5 | 19.4 | 299.9 | 17.9 |
| | $1.0E-03$ | 50.1 | 19.4 | 299.9 | 17.5 |
| | $1.0E-02$ | 50.0 | 20.7 | 299.8 | 18.5 |
| 5 | $1.0E-04$ | 44.9 | 32.4 | 269.8 | 29.6 |
| | $5.0E-04$ | 50.4 | 32.5 | 299.2 | 28.9 |
| | $7.5E-04$ | 49.7 | 32.3 | 299.4 | 29.3 |
| | $1.0E-03$ | 49.7 | 32.1 | 299.8 | 29.3 |
| | $1.0E-02$ | 49.2 | 33.9 | 299.4 | 30.6 |
| 10 | $1.0E-04$ | 43.7 | 64.9 | 268.6 | 59.1 |
| | $5.0E-04$ | 47.4 | 63.9 | 298.2 | 58.8 |
| | $7.5E-04$ | 47.8 | 64.8 | 298.4 | 58.6 |
| | $1.0E-03$ | 48.9 | 64.8 | 298.6 | 58.3 |
| | $1.0E-02$ | 47.8 | 67.8 | 297.9 | 62.1 |

the MMF applied to a large set of data points may result in the loss of the detailed information in time of the evolution of the power, therefore an optimization of this parameter is necessary.

The application of KF (with a process noise error $Q = 10^{-6}$) leads to an additional reduction of the standard deviation, as is shown in Table 5, that becomes more visible when situations with a larger noise on the power signal (i.e. larger value of $\delta$)

Table 4
Results of statistical analysis using a Moving Mean Filter over an 11 point span to process the signal affected by noise before applying the reactivity reconstruction method. The transient is induced by an insertion of $\rho_p$ reactivity. $\langle \rho_{p,exp} \rangle$ denotes the sample average of the measured distance between the experimental reactivity $\rho_{exp}$ and the reference configuration $\rho_0 = -2041$ pcm; $\sigma_\rho$ is the corresponding standard deviation. Ten thousand power histories are considered.

| | | $\rho_p = 50$ pcm | | $\rho_p = 300$ pcm | |
|---|---|---|---|---|---|
| $\delta$ [%] | $t$ [s] | $\langle \rho_{p,exp} \rangle$ [pcm] | $\sigma_\rho$ [pcm] | $\langle \rho_{p,exp} \rangle$ [pcm] | $\sigma_\rho$ [pcm] |
| 1 | $1.0E-04$ | 44.3 | 4.5 | 263.1 | 4.1 |
| | $5.0E-04$ | 50.0 | 4.5 | 300.0 | 4.1 |
| | $7.5E-04$ | 50.0 | 4.6 | 300.0 | 4.1 |
| | $1.0E-03$ | 50.0 | 4.5 | 300.0 | 4.0 |
| | $1.0E-02$ | 50.0 | 4.5 | 300.0 | 4.1 |
| 3 | $1.0E-04$ | 44.2 | 13.5 | 262.9 | 12.4 |
| | $5.0E-04$ | 49.9 | 13.5 | 299.9 | 12.2 |
| | $7.5E-04$ | 49.8 | 13.5 | 299.9 | 12.2 |
| | $1.0E-03$ | 50.1 | 13.5 | 300.1 | 12.2 |
| | $1.0E-02$ | 49.8 | 13.8 | 299.8 | 12.5 |
| 5 | $1.0E-04$ | 44.0 | 22.5 | 262.7 | 20.7 |
| | $5.0E-04$ | 49.7 | 22.6 | 299.7 | 20.4 |
| | $7.5E-04$ | 49.8 | 22.8 | 299.8 | 20.6 |
| | $1.0E-03$ | 49.9 | 22.3 | 299.9 | 20.2 |
| | $1.0E-02$ | 49.6 | 22.7 | 299.7 | 20.5 |
| 10 | $1.0E-04$ | 43.2 | 45.1 | 262.0 | 41.4 |
| | $5.0E-04$ | 48.9 | 45.2 | 299.0 | 40.9 |
| | $7.5E-04$ | 49.3 | 45.6 | 299.3 | 41.3 |
| | $1.0E-03$ | 49.5 | 44.7 | 299.5 | 40.4 |
| | $1.0E-02$ | 48.9 | 45.4 | 299.0 | 41.1 |

are considered. However, the corresponding mean value obtained when processing the signal with the Kalman filter shows a small drift, with a partial under-prediction of the reactivity insertion, with respect to the exact value in correspondence to large noise introductions (e.g. $\delta = 10\%$), constituting a partial drawback for the application of this technique. This effect, that has been observed in most of the cases analyzed, can be kept under control with a proper definition of the parameters of the Kalman filter.

Table 5
Results of statistical analysis using the Kalman filter with process noise error $Q = 10^{-6}$ to process the signal affected by noise before applying the reactivity reconstruction method. The transient is induced by an insertion of $\rho_p$ reactivity. $\langle \rho_{p,exp} \rangle$ denotes the sample average of the measured distance between the experimental reactivity $\rho_{exp}$ and the reference configuration $\rho_0 = -2041$ pcm; $\sigma_\rho$ is the corresponding standard deviation. Ten thousand power histories are considered.

| | | $\rho_p = 50$ pcm | | $\rho_p = 300$ pcm | |
|---|---|---|---|---|---|
| $\delta$ [%] | $t$ [s] | $\langle \rho_{p,exp} \rangle$ [pcm] | $\sigma_\rho$ [pcm] | $\langle \rho_{p,exp} \rangle$ [pcm] | $\sigma_\rho$ [pcm] |
| 1 | $1.0E-04$ | 34.9 | 5.5 | 203.5 | 4.9 |
| | $5.0E-04$ | 49.7 | 5.6 | 299.6 | 5.0 |
| | $7.5E-04$ | 49.8 | 5.7 | 299.9 | 5.0 |
| | $1.0E-03$ | 49.8 | 5.6 | 299.9 | 5.0 |
| | $1.0E-02$ | 49.9 | 5.7 | 299.8 | 5.0 |
| 3 | $1.0E-04$ | 29.8 | 15.0 | 181.2 | 13.6 |
| | $5.0E-04$ | 47.0 | 13.4 | 287.4 | 11.9 |
| | $7.5E-04$ | 48.1 | 13.4 | 295.6 | 11.9 |
| | $1.0E-03$ | 48.5 | 13.4 | 297.9 | 11.9 |
| | $1.0E-02$ | 48.4 | 13.4 | 298.6 | 12.0 |
| 5 | $1.0E-04$ | 26.8 | 24.8 | 176.5 | 22.5 |
| | $5.0E-04$ | 42.9 | 20.6 | 276.9 | 18.4 |
| | $7.5E-04$ | 44.5 | 20.8 | 287.6 | 18.6 |
| | $1.0E-03$ | 45.2 | 20.9 | 292.3 | 18.6 |
| | $1.0E-02$ | 45.6 | 21.0 | 296.2 | 18.8 |
| 10 | $1.0E-04$ | 14.0 | 49.9 | 163.6 | 45.4 |
| | $5.0E-04$ | 28.9 | 40.1 | 258.8 | 35.9 |
| | $7.5E-04$ | 30.6 | 39.8 | 269.2 | 35.6 |
| | $1.0E-03$ | 31.4 | 39.4 | 274.6 | 35.4 |
| | $1.0E-02$ | 32.6 | 39.6 | 284.2 | 35.6 |

The Monte Carlo analysis presented allows to assess the potentialities of the different filtering approaches in improving the reactivity predictions in the presence of noisy data. Nevertheless, the analysis and interpretation of a single power history allows to get an idea on what can be expected in an experimental observation of a specific power evolution. To this aim, the calculated power signal is elaborated adding the noise contribution as before, and the same sequence of noisy data points

is interpreted introducing the proposed filtering techniques. The results obtained are reported in Figs. 3 and 4, allowing a graphical comparison of the behavior of the reactivity. A perturbation of $300$ pcm is considered and two values of $\delta$ are adopted, $3\%$ and $10\%$, thus representing the same cases as reported in the previous tables. The observation of these graphs confirms the previous comments: all the filtering methods are effective in reducing the dispersion of the reactivity results, and the correct tuning of the filtering parameters (number of points in MMF and the process error $Q$ for KF) allows to minimize the drifting effect.

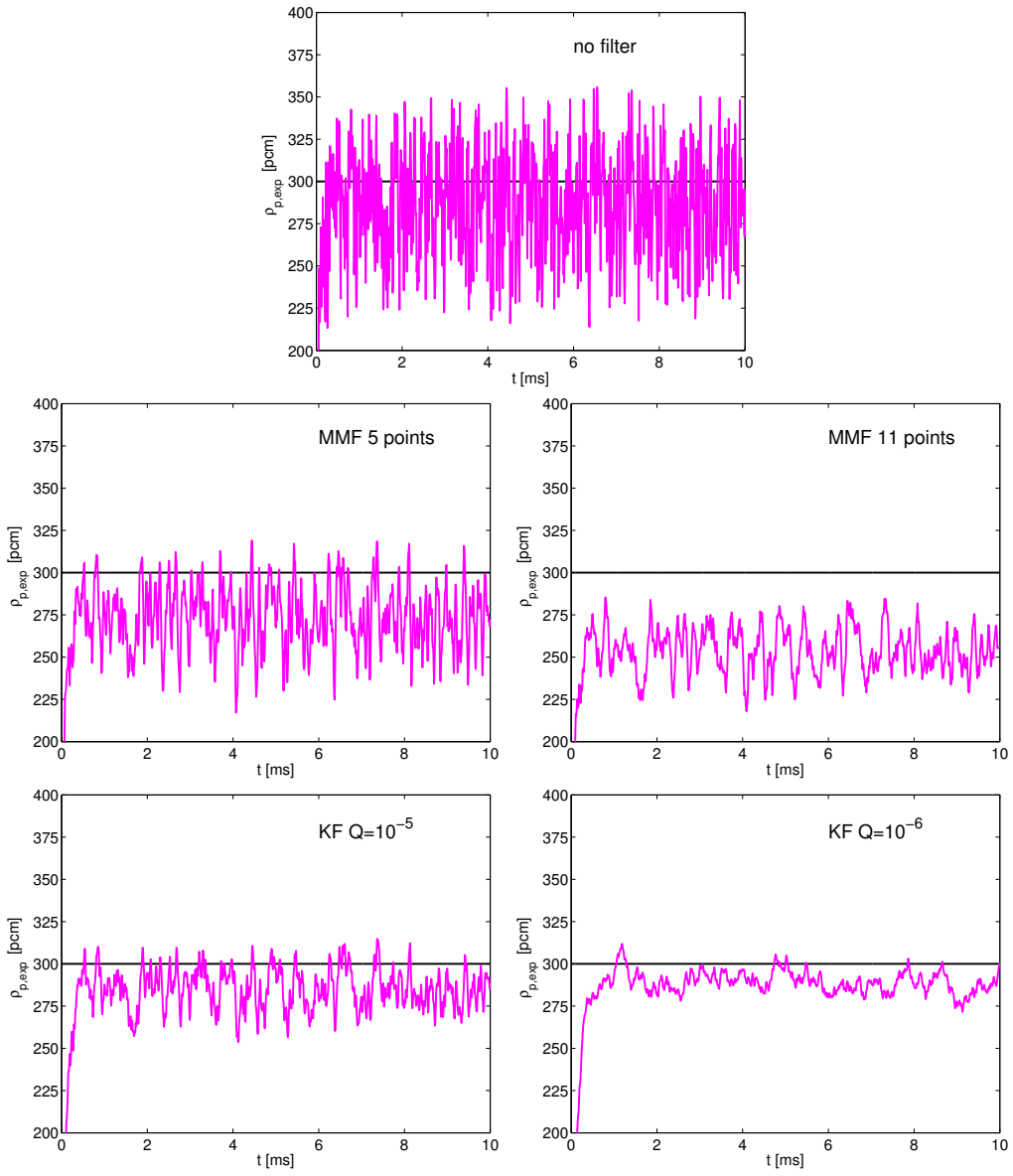


Figure 3. Result of the application of the reactivity reconstruction algorithm to a noisy power signal ($\delta = 3\%$) adopting different filtering techniques. Top graph: no filter; center graphs: MMF with 5 points (left) and 11 points (right); bottom graphs: KF with $Q = 10^{-5}$ (left) and $Q = 10^{-6}$ (right). Black line refers to the exact reactivity value.

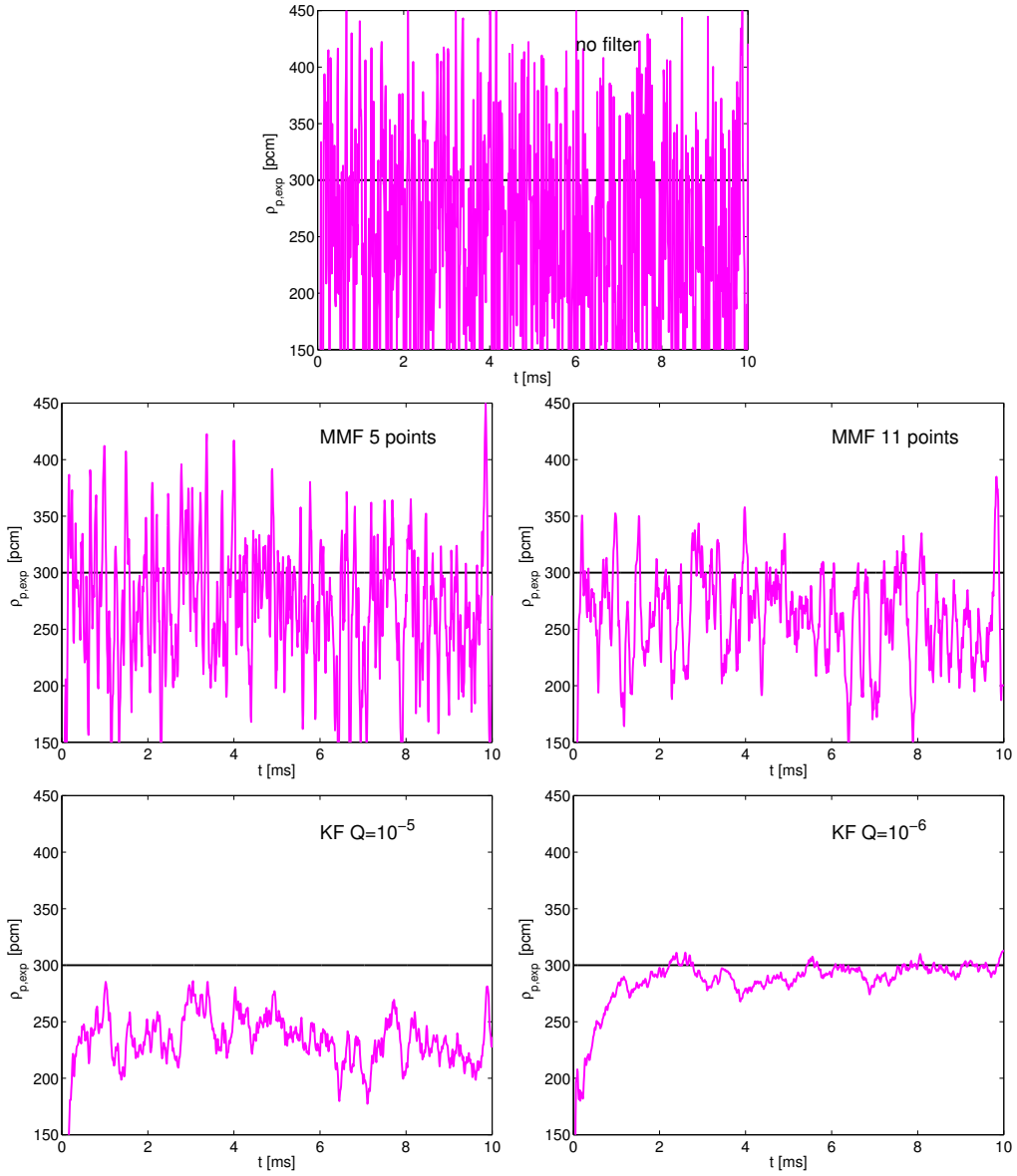


Figure 4. Result of the application of the reactivity reconstruction algorithm to a noisy power signal ($\delta = 10\%$) adopting different filtering techniques. Top graph: no filter; center graphs: MMF with 5 points (left) and 11 points (right); bottom graphs: KF with $Q = 10^{-5}$ (left) and $Q = 10^{-6}$ (right). Black line refers to the exact reactivity value.

## 5 Spatial and spectral effects

In the previous sections the method has been tested using a point kinetic model to simulate experimental power signals and the effect of the experimental noise has been computationally simulated. In real experiments the information on the evolution of the system is retrieved by flux measurements at specific detector positions inside the reactor system. Such measurements are influenced by the type of detector, which determines its energy spectrum efficiency, and by the detector location, which may introduce relevant spatial effects. The aim of this section is to interpret flux signals, in order to characterize the performance and robustness of the method when spatial and spectral effects are present. Again, these signals are generated by a diffusion code, which solves the time-dependent multigroup diffusion equations numerically (Dulla et al., 2013). Only one family of delayed neutron precursors is assumed. The effective delayed neutron fraction and the mean generation time are here evaluated by the classical formulae, based on adjoint-weighted integration, consistently with the point kinetic model (Akcasu et al., 1971).

Figure 5 presents the geometry of the one-dimensional configuration considered for this investigation on spatial and spectral effects. The system is characterized by material data typical of a lead-cooled fast reactor (Dulla et al., 2013). Two different energy-space localized perturbations (identified by P1 and P2) and 4 and 49 energy structures (Dulla et al., 2013) are considered to test the reactivity reconstruction technique. In Table 6 the group structure for the 4-group and 49-group cases is reported. The choice of 49 groups refers to the built-in energy grids that are available in the ERANOS code (Rimpault et al., 2002); the 49 groups have been obtained using the standard 33 group structure below 0.82 MeV and the finest 172 group structure above this energy (Bianchini et al., 2010). In Fig. 5 also the position of four detectors is indicated (DET1 through DET4). At each position the detector can be associated to each of the energy groups considered. The physical parameters and the perturbation features are listed in Table 7. In order to simplify the computational algorithm, only one family of precursors is considered. In other works, where the interpretation method has been applied to real experimental data (Dulla et al., 2014d) or to coupled calculations for lead-cooled fast reactors (Caron et al., 2014), a multiple-family set for the delayed neutron precursors has been assumed, to be consistent with the flux signals analyzed. In the results here presented, the use of one family does not affect the overall validity of the method since the same data are used in both the generation of the signals and in their interpretation and the present work is focused on the computational assessment of the algorithm.

The perturbed region is affected for the 4-group case by a change of the fission cross section in the second energy group, and in the 49-group case by a change of the fission cross section in all groups from 8 through 25, that are collapsed into group 2 in the 4-group case. The 14 MeV source emissions appear in the first energy group for the 4-energy group case, while for the 49 energy structure the source emissions

take place in the third group.

Results of the reactivity predictions starting from the signals at the various detectors during the transients induced by both perturbations are reported in Table 8 through 15. Also the prediction yielded by the power signal (usually not readily available in practical situations) is shown in Tables 8 and 12.

Considering the perturbation P1, it is clear that DET1 is strongly affected by the presence of the source and also by the phenomena due to the material perturbation. The most accurate reactivity estimation can be retrieved by the flux signals of DET2: it is located in the center of the fuel region in such a way to be capable to gain good information of the system evolution, without being unfavorably affected by spatial and spectral source effects. Not very accurate results are obtained by interpreting the flux signals for the first energy group in DET1 through DET3, because of the effect of the energy spectrum of the source, injecting neutrons directly in the first group. Therefore, the signal is affected by neutrons coming directly from the source and, hence, with little information on the multiplication properties of the system. The first energy group flux signal in DET4 gives better results. This can be due to its location inside the reflector and not very close to the source and thus not dominated by uncollided neutrons. In any case, the reactivity estimation errors are less than 10 pcm.

Interpreting the transient induced by the perturbation P2, the same considerations about the DET1 behavior can be drawn. In this configuration the most precise reactivity estimation is obtained by the signals of the DET3, which is the closest to the perturbed region. For both P1 and P2 the prediction improves when interpreting the signal from the fourth energy group neutrons, since such particles gain a deeper knowledge of the characteristics of the system from a larger number of interactions.

The same system is also studied considering a 49-energy group grid in order to more deeply investigate the spectral features of the problem. Figures 6 and 7 present the results obtained for all the detectors at different time instants for both perturbations P1 and P2. In both cases better performances are obtained for signals taken in the intermediate energy section, not directly affected by the source emissions; poor results are also expected in the soft spectrum range, that is little representative of the system multiplying characteristics. In the intermediate energy region, the accuracy is of the order of 20 pcm. These effects are attenuated as early as $10^{-3}$s after the initiation of the transient, allowing to reach the same accuracy of the intermediate energy group regions.

The results here presented enlighten the importance of spatial and spectral effects and how they can affect the quality of the reactivity reconstruction, being based on a point-like approach. Various techniques for the correction of the reactivity obtained by the analysis of local flux measurements have been proposed in conjunction with other interpretation methods (Salvatores et al., 1996; Persson et al.,

2005), usually acting on the output values obtained in order to reduce their discrepancies. Recently, an alternative approach for the reduction of spatial and spectral effects in the application of the present interpretation method has been developed (Dulla et al., 2014a), based on a weighting procedure of the flux signals on the corresponding adjoint function, thus allowing to correctly represent the importance of the different contributions in the representation of the global behaviour of the system.

All the results presented in this section regard transients induced by step perturbation of cross sections as generated by a numerical code to mimic experimental measurements. The method has been proven to work effectively also in the case of a time-dependent reactivity, as in the analysis of coupled neutronics/thermalhydraulics transients (Caron et al., 2014).

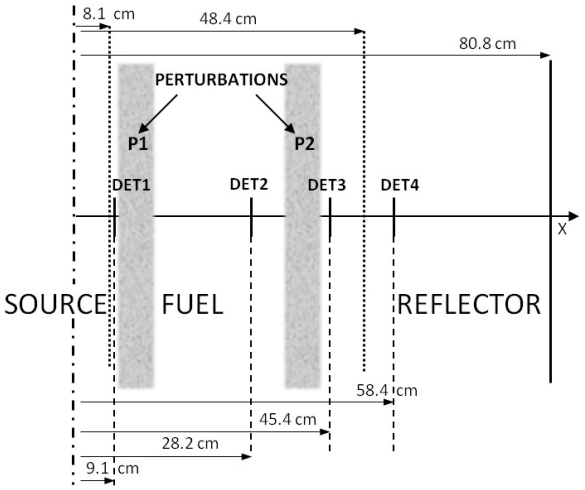


Figure 5. Geometrical configuration of the system for the study of the spatial and spectral effects. The grey perturbed regions (P1, P2) are affected by a change of the fission cross section. The positions of the flux detectors are also indicated.

Table 6
Multigroup energy structure.

| Upper energy boundary [MeV] | 4-group | 49-group |
|---|---|---|
| 19.64 | 1 | $1-7$ |
| 8 | 2 | $8-25$ |
| 0.3 | 3 | $26-27$ |
| 0.188 | 4 | $28-49$ |

Table 7
Data adopted for the analysis of spatial effects for the 4 and 49 energy group cases.

| | 4-Energy groups | | 49-Energy groups | |
|---|---|---|---|---|
| $\Lambda$ [s] | $9.02E-07$ | | $4.20E-07$ | |
| $\beta$ [pcm] | 732.69 | | 718.7 | |
| $\lambda$ [s$^{-1}$] | 0.1 | | 0.1 | |
| $\rho_0$ [pcm] | $-2041$ | | $-2041$ | |
| | P1 | P2 | P1 | P2 |
| $\rho_p$ [pcm] | 299.34 | 319.02 | 261.92 | 195.91 |
| $\delta\Sigma_f$ [%] | 5 | 8 | 3 | 5 |

Table 8
Performance of the interpretation technique for detector DET1 in the case of perturbation P1 in the 4-group case. Results from the interpretation of the total power is also shown, proving that more accurate results are to be expected. Column headings $\Phi_g$ indicate that the flux $\Phi_g$ is used as input signal to the interpretation algorithm. The same for the following Tables.

| $t$ | | $(\rho_{exp}-\rho)$ [pcm] | | | |
|---|---|---|---|---|---|
| $[s]$ | Power | $\Phi_1$ | $\Phi_2$ | $\Phi_3$ | $\Phi_4$ |
| $1.00E-05$ | $5.7E+00$ | $-2.8E+02$ | $4.3E+00$ | $2.3E+00$ | $3.3E+00$ |
| $1.00E-04$ | $7.0E+00$ | $-2.8E+02$ | $3.7E+00$ | $2.1E+00$ | $1.1E+00$ |
| $1.00E-03$ | $7.8E+00$ | $-2.8E+02$ | $4.5E+00$ | $2.8E+00$ | $1.9E+00$ |
| $1.00E-02$ | $7.8E+00$ | $-2.8E+02$ | $4.5E+00$ | $2.8E+00$ | $1.9E+00$ |
| $1.00E-01$ | $7.8E+00$ | $-2.8E+02$ | $4.5E+00$ | $2.8E+00$ | $1.9E+00$ |
| 1 | $7.8E+00$ | $-2.8E+02$ | $4.2E+00$ | $2.7E+00$ | $2.0E+00$ |
| 1.5 | $7.8E+00$ | $-2.8E+02$ | $4.1E+00$ | $2.7E+00$ | $2.0E+00$ |
| 2 | $7.8E+00$ | $-2.8E+02$ | $4.0E+00$ | $2.6E+00$ | $2.0E+00$ |
| 5 | $7.8E+00$ | $-2.8E+02$ | $3.4E+00$ | $2.4E+00$ | $2.1E+00$ |
| 10 | $7.8E+00$ | $-2.8E+02$ | $2.7E+00$ | $2.1E+00$ | $2.2E+00$ |

Table 9
Performance of the interpretation technique for detector DET2 in the case of perturbation P1 in the 4-group case.

| $t$ | $(\rho_{exp} - \rho)$ [pcm] | | | |
|---|---|---|---|---|
| $[s]$ | $\Phi_1$ | $\Phi_2$ | $\Phi_3$ | $\Phi_4$ |
| $1.00E-05$ | $-7.4E+01$ | $-1.8E+00$ | $-1.7E+00$ | $-2.4E+00$ |
| $1.00E-04$ | $-6.8E+01$ | $-1.2E-01$ | $-1.5E-01$ | $-6.1E-01$ |
| $1.00E-03$ | $-6.7E+01$ | $6.9E-01$ | $6.6E-01$ | $2.4E-01$ |
| $1.00E-02$ | $-6.7E+01$ | $6.9E-01$ | $6.6E-01$ | $2.3E-01$ |
| $1.00E-01$ | $-6.7E+01$ | $7.1E-01$ | $6.9E-01$ | $2.6E-01$ |
| $1$ | $-6.7E+01$ | $9.4E-01$ | $9.2E-01$ | $5.0E-01$ |
| $1.5$ | $-6.7E+01$ | $1.1E+00$ | $1.0E+00$ | $6.4E-01$ |
| $2$ | $-6.7E+01$ | $1.2E+00$ | $1.2E+00$ | $7.6E-01$ |
| $5$ | $-6.6E+01$ | $1.8E+00$ | $1.7E+00$ | $1.4E+00$ |
| $10$ | $-6.5E+01$ | $2.4E+00$ | $2.4E+00$ | $2.1E+00$ |

Table 10
Performance of the interpretation technique for detector DET3 in the case of perturbation P1 in the 4-group case.

| $t$ | $(\rho_{exp} - \rho)$ [pcm] | | | |
|---|---|---|---|---|
| $[s]$ | $\Phi_1$ | $\Phi_2$ | $\Phi_3$ | $\Phi_4$ |
| $1.00E-05$ | $-1.8E+01$ | $-7.4E+00$ | $-6.4E+00$ | $-1.2E+01$ |
| $1.00E-04$ | $-1.2E+01$ | $-2.7E+00$ | $-2.5E+00$ | $-2.3E+00$ |
| $1.00E-03$ | $-1.1E+01$ | $-1.8E+00$ | $-1.7E+00$ | $-1.4E+00$ |
| $1.00E-02$ | $-1.1E+01$ | $-1.8E+00$ | $-1.7E+00$ | $-1.4E+00$ |
| $1.00E-01$ | $-1.1E+01$ | $-1.8E+00$ | $-1.6E+00$ | $-1.4E+00$ |
| $1$ | $-1.0E+01$ | $-1.4E+00$ | $-1.2E+00$ | $-9.8E-01$ |
| $1.5$ | $-1.0E+01$ | $-1.1E+00$ | $-9.9E-01$ | $-7.7E-01$ |
| $2$ | $-1.0E+01$ | $-9.2E-01$ | $-7.9E-01$ | $-5.8E-01$ |
| $5$ | $-9.0E+00$ | $1.5E-01$ | $2.6E-01$ | $4.1E-01$ |
| $10$ | $-7.9E+00$ | $1.3E+00$ | $1.4E+00$ | $1.5E+00$ |

Table 11
Performance of the interpretation technique for detector DET4 in the case of perturbation P1 in the 4-group case.

| $t$ | $(\rho_{exp} - \rho)$ [pcm] | | | |
|---|---|---|---|---|
| $[s]$ | $\Phi_1$ | $\Phi_2$ | $\Phi_3$ | $\Phi_4$ |
| $1.00E-05$ | $-1.7E+01$ | $-7.6E+00$ | $-6.9E+00$ | $-6.1E+01$ |
| $1.00E-04$ | $-1.1E+01$ | $-2.8E+00$ | $-2.7E+00$ | $-2.7E+00$ |
| $1.00E-03$ | $-9.7E+00$ | $-1.9E+00$ | $-1.8E+00$ | $-1.7E+00$ |
| $1.00E-02$ | $-9.7E+00$ | $-1.9E+00$ | $-1.8E+00$ | $-1.7E+00$ |
| $1.00E-01$ | $-9.7E+00$ | $-1.9E+00$ | $-1.7E+00$ | $-1.6E+00$ |
| $1$ | $-9.3E+00$ | $-1.4E+00$ | $-1.3E+00$ | $-1.2E+00$ |
| $1.5$ | $-9.1E+00$ | $-1.2E+00$ | $-1.1E+00$ | $-1.0E+00$ |
| $2$ | $-8.9E+00$ | $-9.8E-01$ | $-8.9E-01$ | $-8.0E-01$ |
| $5$ | $-8.0E+00$ | $9.6E-02$ | $1.7E-01$ | $2.4E-01$ |
| $10$ | $-6.9E+00$ | $1.3E+00$ | $1.3E+00$ | $1.4E+00$ |

Table 12
Performance of the interpretation technique for detector DET1 in the case of perturbation P2 in the 4-group case. Results from the interpretation of the total power is also shown, proving that more accurate results are to be expected.

| $t$ | $(\rho_{exp} - \rho)$ [pcm] | | | | |
|---|---|---|---|---|---|
| [s] | Power | $\Phi_1$ | $\Phi_2$ | $\Phi_3$ | $\Phi_4$ |
| $1.00E-05$ | $-1.4E+01$ | $-2.7E+02$ | $-4.9E+01$ | $-4.4E+01$ | $-3.9E+01$ |
| $1.00E-04$ | $-7.9E+00$ | $-2.7E+02$ | $-4.1E+01$ | $-3.7E+01$ | $-3.2E+01$ |
| $1.00E-03$ | $-7.0E+00$ | $-2.7E+02$ | $-4.0E+01$ | $-3.6E+01$ | $-3.1E+01$ |
| $1.00E-02$ | $-7.0E+00$ | $-2.7E+02$ | $-4.0E+01$ | $-3.6E+01$ | $-3.1E+01$ |
| $1.00E-01$ | $-7.0E+00$ | $-2.7E+02$ | $-4.0E+01$ | $-3.6E+01$ | $-3.1E+01$ |
| $1$ | $-7.1E+00$ | $-2.7E+02$ | $-4.0E+01$ | $-3.6E+01$ | $-3.0E+01$ |
| $1.5$ | $-7.1E+00$ | $-2.7E+02$ | $-3.9E+01$ | $-3.5E+01$ | $-3.0E+01$ |
| $2$ | $-7.1E+00$ | $-2.7E+02$ | $-3.9E+01$ | $-3.5E+01$ | $-3.0E+01$ |
| $5$ | $-7.2E+00$ | $-2.7E+02$ | $-3.8E+01$ | $-3.4E+01$ | $-2.9E+01$ |
| $10$ | $-7.3E+00$ | $-2.7E+02$ | $-3.7E+01$ | $-3.3E+01$ | $-2.7E+01$ |

Table 13
Performance of the interpretation technique for detector DET2 in the case of perturbation P2 in the 4-group case.

| $t$ | $(\rho_{exp} - \rho)$ [pcm] | | | |
|---|---|---|---|---|
| [s] | $\Phi_1$ | $\Phi_2$ | $\Phi_3$ | $\Phi_4$ |
| $1.00E-05$ | $-8.5E+01$ | $-2.1E+01$ | $-2.2E+01$ | $-2.3E+01$ |
| $1.00E-04$ | $-7.7E+01$ | $-1.5E+01$ | $-1.6E+01$ | $-1.7E+01$ |
| $1.00E-03$ | $-7.6E+01$ | $-1.4E+01$ | $-1.5E+01$ | $-1.6E+01$ |
| $1.00E-02$ | $-7.6E+01$ | $-1.4E+01$ | $-1.5E+01$ | $-1.6E+01$ |
| $1.00E-01$ | $-7.6E+01$ | $-1.4E+01$ | $-1.5E+01$ | $-1.6E+01$ |
| 1 | $-7.5E+01$ | $-1.4E+01$ | $-1.5E+01$ | $-1.6E+01$ |
| 1.5 | $-7.5E+01$ | $-1.4E+01$ | $-1.4E+01$ | $-1.5E+01$ |
| 2 | $-7.5E+01$ | $-1.4E+01$ | $-1.4E+01$ | $-1.5E+01$ |
| 5 | $-7.5E+01$ | $-1.3E+01$ | $-1.4E+01$ | $-1.5E+01$ |
| 10 | $-7.4E+01$ | $-1.3E+01$ | $-1.3E+01$ | $-1.4E+01$ |

Table 14
Performance of the interpretation technique for detector DET3 in the case of perturbation P2 in the 4-group case.

| $t$ | $(\rho_{exp} - \rho)$ [pcm] | | | |
|---|---|---|---|---|
| [s] | $\Phi_1$ | $\Phi_2$ | $\Phi_3$ | $\Phi_4$ |
| $1.00E-05$ | $1.8E+01$ | $1.6E+01$ | $5.0E+00$ | $-6.8E+00$ |
| $1.00E-04$ | $2.2E+01$ | $2.0E+01$ | $9.5E+00$ | $8.2E-02$ |
| $1.00E-03$ | $2.2E+01$ | $2.0E+01$ | $1.0E+01$ | $9.0E-01$ |
| $1.00E-02$ | $2.2E+01$ | $2.0E+01$ | $1.0E+01$ | $8.9E-01$ |
| $1.00E-01$ | $2.2E+01$ | $2.0E+01$ | $1.0E+01$ | $8.9E-01$ |
| 1 | $2.2E+01$ | $2.0E+01$ | $9.9E+00$ | $8.2E-01$ |
| 1.5 | $2.1E+01$ | $1.9E+01$ | $9.8E+00$ | $7.9E-01$ |
| 2 | $2.1E+01$ | $1.9E+01$ | $9.6E+00$ | $7.7E-01$ |
| 5 | $1.9E+01$ | $1.8E+01$ | $9.0E+00$ | $6.3E-01$ |
| 10 | $1.6E+01$ | $1.6E+01$ | $8.2E+00$ | $4.6E-01$ |

Table 15
Performance of the interpretation technique for detector DET4 in the case of perturbation P2 in the 4-group case.

| $t$ | $(\rho_{exp} - \rho)$ [pcm] | | | |
|---|---|---|---|---|
| [s] | $\Phi_1$ | $\Phi_2$ | $\Phi_3$ | $\Phi_4$ |
| $1.00E-05$ | $1.6E+01$ | $1.5E+01$ | $9.3E+00$ | $-1.4E+01$ |
| $1.00E-04$ | $2.0E+01$ | $1.9E+01$ | $1.4E+01$ | $9.2E+00$ |
| $1.00E-03$ | $2.1E+01$ | $2.0E+01$ | $1.4E+01$ | $1.0E+01$ |
| $1.00E-02$ | $2.1E+01$ | $2.0E+01$ | $1.4E+01$ | $1.0E+01$ |
| $1.00E-01$ | $2.0E+01$ | $2.0E+01$ | $1.4E+01$ | $1.0E+01$ |
| 1 | $2.0E+01$ | $1.9E+01$ | $1.4E+01$ | $9.7E+00$ |
| 1.5 | $1.9E+01$ | $1.9E+01$ | $1.4E+01$ | $9.6E+00$ |
| 2 | $1.9E+01$ | $1.9E+01$ | $1.3E+01$ | $9.4E+00$ |
| 5 | $1.7E+01$ | $1.7E+01$ | $1.3E+01$ | $8.8E+00$ |
| 10 | $1.5E+01$ | $1.6E+01$ | $1.2E+01$ | $8.0E+00$ |

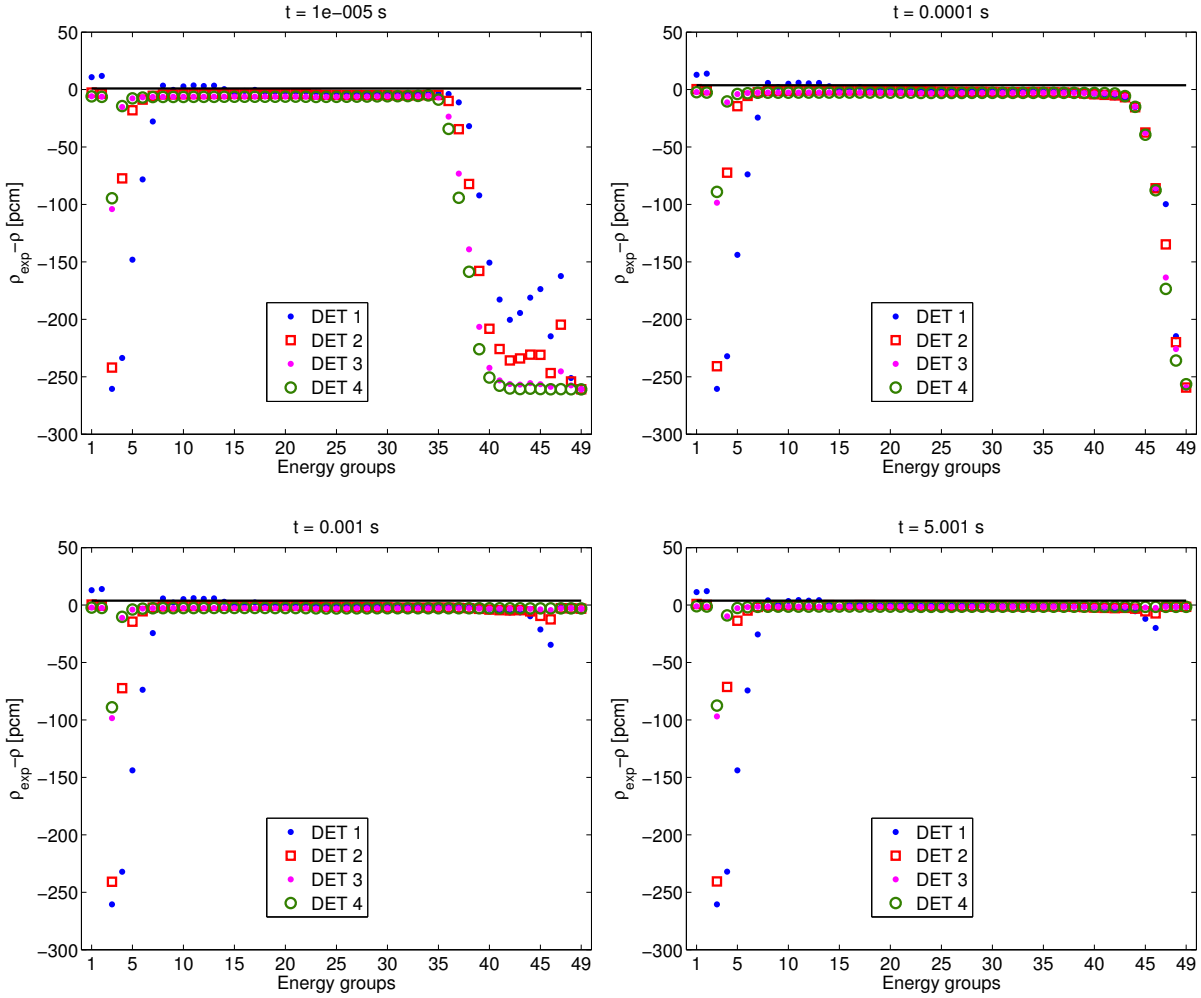


Figure 6. Accuracy of the reactivity prediction for space and energy neutron detectors at various instants following the introduction of perturbation P1 in the 49-group case.

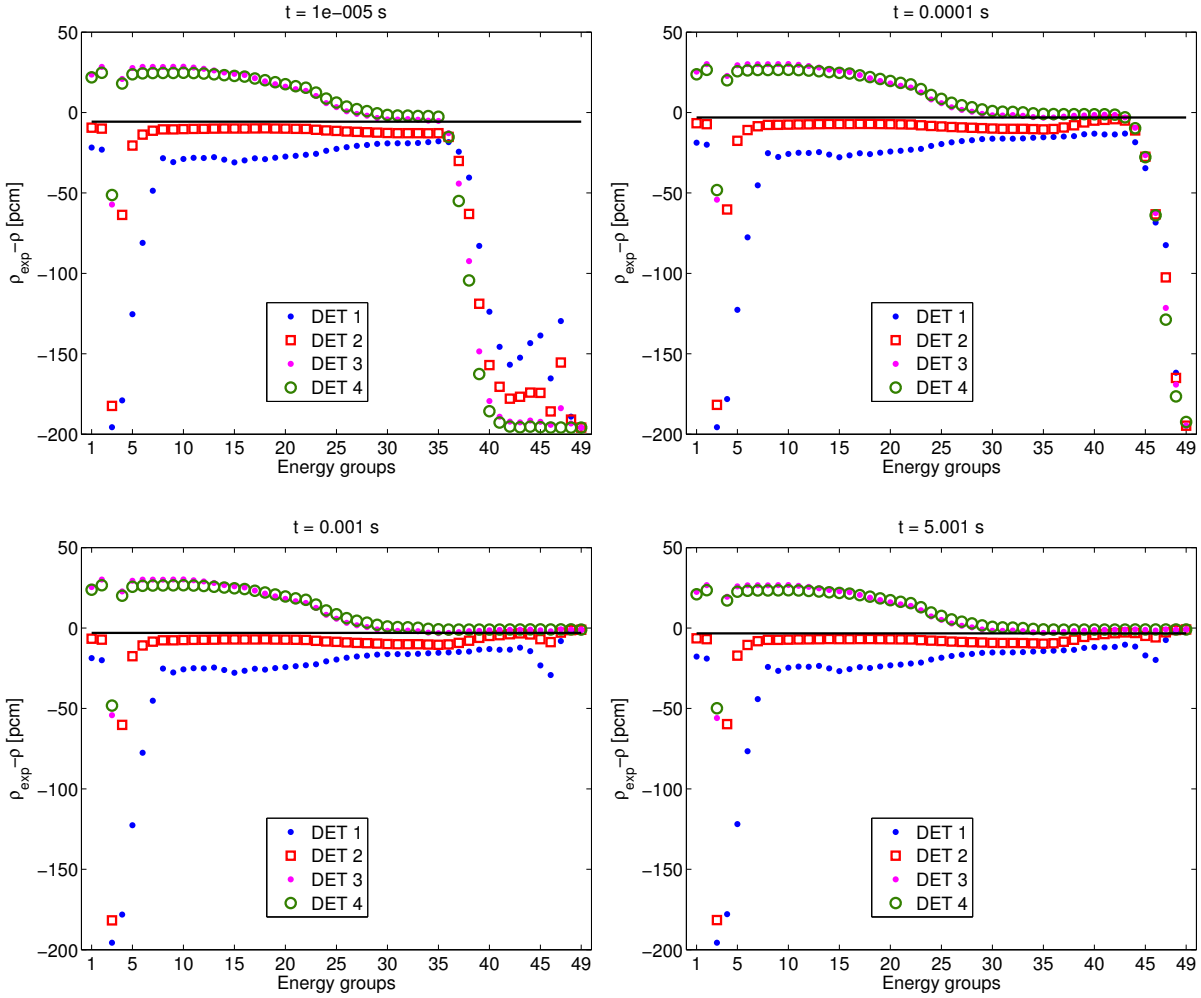


Figure 7. Accuracy of the reactivity prediction for space and energy neutron detectors at various instants following the introduction of perturbation P2 in the 49-group case.

## 6 Conclusions and future developments

A novel on-line reactivity monitoring technique based on the point kinetic equations is presented and assessed for application to source-driven systems. The method is applied to analyse the evolutions in several different transient conditions, proving its capability to promptly and accurately detect the reactivity changes introduced into the system. A sensitivity analysis allows to study and quantify the effects of the uncertainties affecting the kinetic parameters, which are supposed to be available from independent measurements or evaluations.

The robustness of the method is investigated by investigating its suitability to deal with noisy signals. It is shown that adequate results are obtained by using an appropriate differentiation procedure together with noise reduction filtering techniques. The spatial and spectral effects are also investigated. In future works the possibility to introduce proper correction techniques to compensate for spatial and spectral distortions will be considered.

The results obtained give enough confidence on the capability of the method to yield satisfactory performances when applied to real configurations. Future works will be focused on the application of the method to the analysis of real experiments.

## Acknowledgments

Part of this work is included in the activities of IAEA Collaboration Work on Accelerator Driven System (ADS) and Use of Low Enriched Uranium (LEU) in ADS.

## References

Akcasu, Z., Lellouche, G., Shotkin, L., 1971. *Mathematical methods in nuclear reactor dynamics*. Academic Press, New York.

Baeten, P., Paepen, J., van der Meer, K., Aït Abderrahim, H., 2001. Absolute measurement of $\beta_{eff}$ and $l$ on weapon-grade mox fuel at the VENUS critical facility by means of the RAPJA technique. *Annals of Nuclear Energy* **28**, 287–295.

Becares, V., Villamarín, D., Fernandez-Ordonez, M., Gonzalez-Romero, E., Berglof, C., Bournos, V., Fokov, Y., Mazanik, S., I., S., 2013. Validation of ADS reactivity monitoring techniques in the yalina-booster subcritical assembly. *Annals of Nuclear Energy* **53**, 331–341.

Bianchini, G., Carta, M., Pisacane, F., Frisoni, M., Peluso, V., 2010. Set-up of a deterministic model for the analysis of the GUINEVERE experience, in: *Proceedings of the International Conference PHYSOR 2010*, Pittsburgh, PA.

Cao, Y., Gohar, Y., Zhong, Z., 2013. Numerical studies of the flux-to-current ratio method in the kipt neutron source facility, in: *Proceedings of the International Conference on Mathematics and Computational Methods Applied to Nuclear Science and Engineering, M&C 2013*, Sun Valley, ID.

Caron, D., Dulla, S., Nervo, M., Ravetto, P., Carta, M., 2014. Assessment of and on-line reactivity monitoring technique. *Transactions on the American Nuclear Society* **111**, 1185–1187.

Chartrand, R., 2011. Numerical differentiation of noisy, nonsmooth data. *ISRN Applied Mathematics* **2011**, doi:10.5402/2011/164564.

Corno, S., Ravetto, P., Sumini, M., 1986. Sulla prevedibilità del valore effettivo del periodo stabile di un reattore nucleare, in: *Proceedings of the 8-th National Congress of the Italian Association of Theoretical and Applied Mechanics (in Italian)*, pp. 667–673.

Dulla, S., Hoh, S.S., Nervo, M., Ravetto, P., 2014a. Reduction of spatial and spectral effects by adjoint weighting of flux signals in a reactivity reconstruction technique. *Transactions on the American Nuclear Society* **111**, 1200–1203.

Dulla, S., Nervo, M., Ravetto, P., 2014b. A method for on-line reactivity monitoring in nuclear reactors. *Annals of Nuclear Energy* **65**, 433 – 440.

Dulla, S., Nervo, M., Ravetto, P., 2014c. A method for reactivity monitoring in subcritical source-driven systems, in: *Proceedings of the International Conference PHYSOR 2014*, Kyoto, Japan.

Dulla, S., Nervo, M., Ravetto, P., Carta, M., 2013. Spatial and spectral effects in subcritical system pulsed experiments, in: *Proceedings of the International Conference on Mathematics and Computational Methods Applied to Nuclear Science and Engineering, M&C 2013*, Sun Valley, ID.

Dulla, S., Nervo, M., Ravetto, P., Mila, G., Argiró, S., Beolé, S., Masera, M., Bianchini, G., Carta, M., Fabrizio, V., Peluso, V., Gabrielli, F., Rineiski, A., Kochetkov, A., Baeten, P., Uyttenhove, W., Vittiglio, G., Wagemans, J., 2014d. Interpretation of experimental measurements on the SC-1 configuration of the VENUS-F core, in: *Proceedings of the International Conference PHYSOR 2014*, Kyoto, Japan.

Kalman, R., 1960. A new approach to linear filtering and prediction problems. *Transactions of the ASME Journal of Basic Engineering* **82**, 35 – 45.

Krilov, A., 1931. The numerical solution of equations determining the frequency of small vibration in material systems in engineering. *Izvestiya Akademii Nauk S.S.S.R.* , 491–539.

Kuramoto, R., dos Santos, A., Jerez, R., Diniz, R., 2007. Absolute measurement of $\beta_{eff}$ based on feynman-$\alpha$ experiments and the two-region model in the IPEN/MB-01 research reactor. *Annals of Nuclear Energy* **34**, 433–442.

Pepyolyshev, Y., 2008. Method of experimental estimation of the effective delayed neutron fraction and of the neutron generation lifetime in the IBR-2 pulsed reactor. *Annals of Nuclear Energy* **35**, 1301–1305.

Persson, C.M., Seltborg, P., Ahlander, A., Gudowski, W., Stummer, T., Kiyavitskaya, H., Bournos, V., Fokov, Y., Serafimovich, I., Chigrinov, S., 2005. Analysis of reactivity determination methods in the subcritical experiment yalina.

*Nuclear Instruments and Methods in Physics Research Section A: Accelerators, Spectrometers, Detectors and Associated Equipment* **554**, 374 – 383.

Ravetto, P., 1997. Reactivity oscillations in a point reactor. *Annals of Nuclear Energy* **33**, 303–314.

Rimpault, G., Plisson, D., Tommasi, J., Jacqmin, R., Rieunier, J.M., Verrier, D., Biron, D., 2002. The ERANOS code and data system for fast reactor neutronic analyses, in: *Proceedings of the International Conference PHYSOR 2002*, Seoul, Korea.

Salvatores, M., Martini, M., Slessarev, I., Soule, R., Cabrillat, J.C., Chauvin, J., Finck, P., Jacqmin, R., Tchistiaakov, A., 1996. MUSE-1: A first experiment at MASURCA to validate the physics of sub-critical multiplying systems relevant to ADS, in: *Proc 2nd Int Conf on Accelerator-Driven Transmutation Technologies and Applications*, Kalmar, Sweden, OECD Nuclear Energy Agency. p. 513.

Savitzky, A., Golay, J.E., 1964. Smoothing and differentiation of data by simplified least squares procedures. *Analytical Chemistry* **36**, 1627 – 1639.

Sjöstrand, N.G., 1956. Measurements on a subcritical reactor using a pulsed neutron source. *Archiv för Fysik* **11**, 233 – 246.